NUCLEIC ACID THERAPEUTICS
Volume 30, Number 6, 2020

DOI: 10.1089/nat.2020.0871

Original Papers

Efficiency and Target Derepression of Anti-miR-92a: Results of a First in Human Study

Wesley Tyler Abplanalp,[1,2,*] Ariane Fischer,[1,*] David John,[1] Andreas M. Zeiher,[2,3] Willy Gosgnach,[4] Helene Darville,[4] Rusty Montgomery,[5] Linda Pestano,[5] Guillaume Allée,[6] Isabelle Paty,[6] Francoise Fougerousse,[6] and Stefanie Dimmeler[1–3]

MicroRNA (miRNA) inhibition is a promising therapeutic strategy in several disease indications. MRG-110 is a locked nucleic acid-based antisense oligonucleotide that targets miR-92a-3p and experimentally was shown to have documented therapeutic effects on cardiovascular disease and wound healing. To gain first insights into the activity of anti-miR-92a in humans, we investigated miR-92a-3p expression in several blood compartments and assessed the effect of MRG-110 on target derepression. Healthy adults were randomly assigned (5:2) to receive a single intravenous dose of MRG-110 or placebo in one of seven sequential ascending intravenous dose cohorts ranging from 0.01 to 1.5 mg/kg body weight. MiR-92a-3p whole blood levels were time and dose dependently decreased with half-maximal inhibition of 0.27 and 0.31 mg/kg at 24 and 72 h after dosing, respectively. In the high-dose groups, >95% inhibition was detected at 24–72 h postinfusion and significant inhibition was observed for 2 weeks. Similar inhibitory effects were detected in isolated $CD31^+$ cells, and miR-92a-3p expression was also inhibited in extracellular vesicles in the high-dose group. Target derepression was measured in whole blood and showed that *ITGA5* and *CD93* were increased at a dose of 1.5 mg/kg. Single-cell RNA sequencing of peripheral blood cells revealed a cell type-specific derepression of miR-92a targets. Together this study demonstrates that systemic infusion of anti-miR-92a efficiently inhibits miR-92a in the peripheral blood compartment and derepresses miR-92a targets in humans.

Keywords: anti-miR, miR-92a, first in human, single cell sequencing

Introduction

MicroRNAs (miRNAs) are a class of short (~22 nt) endogenous noncoding RNAs that mediate post-transcriptional regulation of gene expression. miRNAs play key regulatory roles in various biological processes and are profoundly regulated during pathophysiological conditions. Therefore, miRNAs have emerged as a class of promising targets for therapeutic intervention. miRNAs can be targeted by complementary antisense oligonucleotides, which can be composed of different nucleotides and can be modified by different strategies to increase stability (for review, see Lucas *et al.* [1] and van Rooij and Kauppinen [2]).

Most widely used anti-miRs include ''Antagomirs,'' which are 3′-cholesterol-conjugated, 2′-O-Me, 2′-fluoro, or 2′O-methoxyethyl oligonucleotides, with an additional phosphorothioate backbone [3], or ''locked nucleic acid (LNA)-based anti-miRs,'' in which the second oxygen molecule is linked to the 4′ carbon atom in the ribonucleotide. Locked ribonucleotides are used in combination with deoxyribonucleotides within the anti-miR sequence to create so-called LNA-DNA mixmers [1,2]. LNA-based anti-miRs were shown to be more efficient and were used in large animal models and a first clinical trial, which demonstrates that LNA-based anti-miRs targeting liver miR-122 can be used to treat hepatitis [4].

We and others have demonstrated that inhibition of miR-92a exhibited several beneficial effects in experimental models. MiR-92a belongs to the miR-17-92a cluster and its inhibition by antisense molecules improved vascularization after myocardial infarction and blood circulation after hind limb ischemia, a model of peripheral occlusive disease [5]. Inhibition of miR-92a also leads to accelerated wound healing in animal models with or without metabolic syndrome, which is known to lead to healing disorders [6,7]. Further

[1]Institute for Cardiovascular Regeneration, Goethe University Frankfurt, Frankfurt, Germany.
[2]German Center for Cardiovascular Research (DZHK), Frankfurt, Germany.
[3]Cardio-Pulmonary Institute (CPI), Frankfurt, Germany.
[4]CentEX Biotechnology, Institut de Recherche SERVIER, Paris, France.
[5]miRagen Therapeutics, Inc., Boulder, Colorado, USA.
[6]Center for Therapeutic Innovation Cardiovascular and Metabolic Disease, Institut de Recherches Internationales SERVIER, Paris, France.
*These authors contributed equally to this work.

studies show that anti-miR-92a improves the re-endothelialization after denudation of the endothelium and thus reduces the formation of neointima [8]. MiR-92a knockout mice confirm the protective effect of inhibiting miR-92a in the myocardial infarction model and the prevention of neointima formation after vascular injury [8,9].

In addition, an atheroprotective effect of anti-miR-92a has been described [10], which is presumably due to a reduction in the miR-92a levels increased by oscillating flow in vascular regions with a high predisposition to the development of lesions [11]. The therapeutic utility of miR-92a inhibitors was further confirmed in ischemia/reperfusion model in pigs [12,13]. Here, either infusing encapsulated anti-miR-92a or intracoronary administration of 0.03 mg/kg LNA-based anti-miR-92a significantly improved cardiac function and vascularization. Genetic and pharmacological inhibition of microRNA-92a were further shown to maintain podocyte cell cycle quiescence and limit crescentic glomerulonephritis [14]. Based on this documented, promising therapeutic potential, LNA-based anti-miR-92a was further developed and tested in a first in human study.

Although LNA-based anti-miRs have been shown to be safe and active in human studies of miravirsen, targeting a liver miRNA [4], as well as cobomarsen, targeting miR-155 in multiple hematological malignancies [15], little is known regarding the activity of other anti-miRs in humans. Studying anti-miR activity in humans is challenging, since the biological relevant targets often are regulated in organs, which are not easily accessible. Furthermore, measuring of the targeted miRNA by polymerase chain reaction (PCR) in whole blood may overestimate the biological effects due to possible interference of the remaining anti-miR in the sample with the miRNA measurement. Therefore, we systematically compared the effect of anti-miR-92a treatment in humans on miR-92a expression in several blood compartments. In addition to measuring miR-92a in whole blood, which was technically most reliable, we isolated peripheral blood mononuclear cell (PBMC)-derived $CD31^+$ cells, which are expected to comprise a proportion of circulating endothelial cells, which are one of the primary targets of anti-miR-92a therapeutics. Furthermore, we assessed miR-92a expression in extracellular vesicles (ECV) including exosomes, which are expected to represent exported miRNA levels from circulating immune cells, platelets, and endothelial cells. Target messenger RNAs (mRNAs) were measured in whole blood and $CD31^+$ cells. To determine the cell type-specific response of the anti-miR, we applied single-cell sequencing of peripheral blood cells.

Materials and Methods

This was a single-center, randomized, double-blind, placebo-controlled, dose-escalating study (European Clinical Trials Database [EudraCT] No. 2017-004180-12). All subjects gave their written informed consent, and the Research Ethics Committee approved the study, which was conducted in accordance with good clinical practice guidelines and pertinent legal requirements. Site investigators and participants were masked to the treatment assignment, whereas designated personnel at the site who prepared and generated the study medication were aware of the randomization treatment assignments.

Eligible volunteers were defined as healthy men 18–45 years of age with a body mass index between 18.5 and 30 kg/m^2 and body weight between 50 and 100 kg, nonsmoker or ex-smoker for more than 3 months, with normal liver enzymes laboratory results, with normal fundus oculi assessment and abdominal echography examination performed between the selection and inclusion visits, and with no high myopia or history of high myopia. Participants with a history of dermal/mucosal asymptomatic hemangioma, prior malignancies, and hemangioblastoma could not be included in the study.

Subjects were hospitalized on the day of inclusion (predose) up to day 4 with single administration of placebo or MRG-110 on day 1. This was followed by an ambulatory period of 12 weeks with visits at 2 weeks (W02), 4 weeks (W04), and 12 weeks (W12) after administration.

MRG-110 is 16 nucleotides in length, with base complementarity to the 5′ end of human miRNA, miR-92a-3p. It is a mixmer of LNA and DNA fully modified with phosphorothioate internucleotide linkages. Specific sequence and modification pattern, where lower case is DNA and upper case is LNA, are 5′-CcGggAcAaGTgCAaT-3′.

Subjects were enrolled in seven cohorts of seven participants per dose (five MRG-110 and two placebo), including two sentinel participants per dose (one MRG-110 and one placebo), and receive blindly a single 50-mL intravenous dose of MRG-110 or placebo in one of seven sequential ascending intravenous dose cohorts (0.01, 0.05, 0.15, 0.45, 0.9, 1.2, or 1.5 mg/kg body weight) as a 10-min infusion. MRG-110 solution for infusion was diluted by the clinical center pharmacy staff from a 40-mg/mL sterile solution of MRG-110 (batch No. L0069292) with 0.9% NaCl locally provided. For the matching placebo, 50 mL of the 0.9% NaCl was locally provided. Whole blood was prepared for measurement of miR-92a and its target genes at each visit. ECV and $CD31^+$ cells were isolated at predose and 24 and 72 h in all dose groups and at 2, 4, and 12 weeks in the 0.45 mg to 1.5 mg/kg.

Subjects, consents, and sampling procedure

Whole-blood samples were provided by SGS Belgium with a workflow outlined as in Fig. 1A. In a separate BD vacutainer Mononuclear Cell Preparation Tube containing 0.1 M sodium citrate, blood was collected, centrifuged at 1,500 *g* for 20 min, and then was transported to the Institute of Cardiovascular

FIG. 1. MRG-110 reduces expression of miR-92a-3p in whole blood and isolated $CD31^+$ cells. **(A)** Study design. **(B)** Expression of miR-92a-3p (normalized to mean value of miR-126 and let-7g) in whole blood in subjects treated with a single intravenous dose of MRG-110. $N=5$ in each treatment group, $N=14$ subjects in placebo. $^*P<0.05$ versus placebo. **(C)** Data from **(B)** (24 and 72 h) are shown as dose–response relationship. **(D)** Flow cytometry analysis of negative control (unstained, unsorted PBMCs) and PBMC-derived sorted $CD31^+$ ($FITC^+$) cells. Representative histograms demonstrate $CD31^+$ cell purity. **(E, F)** PBMC counts **(E)** and quality of $CD31^+$ cell-derived RNA (RIN) **(F)** of samples at respective time points. **(G)** Expression of miR-92a-3p (normalized to let-7g) in isolated $CD31^+$ cells of subjects treated with a single intravenous infusion of MRG-110. $N=5$ in each treatment group, $N=14$ subjects in placebo. $^*P<0.05$ versus placebo. **(H)** Data from **(G)** (24 and 72 h) are shown as dose–response relationship. PBMCs, peripheral blood mononuclear cells; RIN, RNA Integrity Number; W, week. Color images are available online.

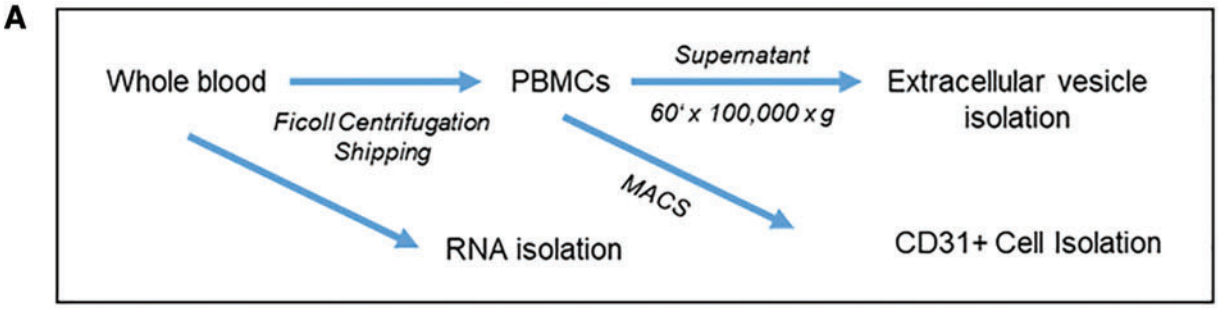

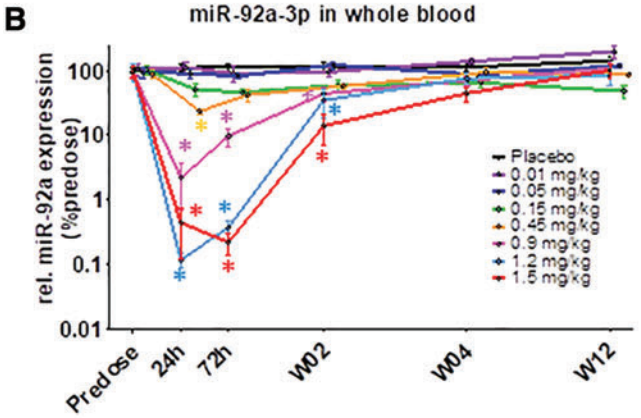

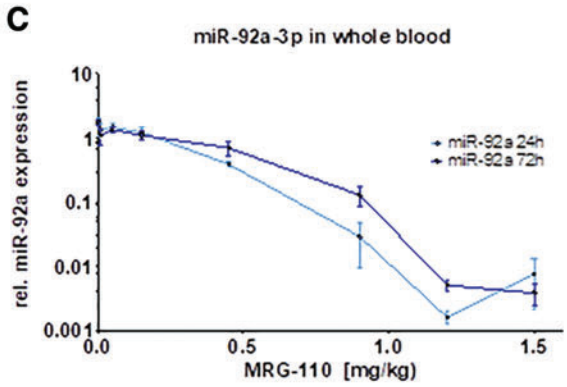

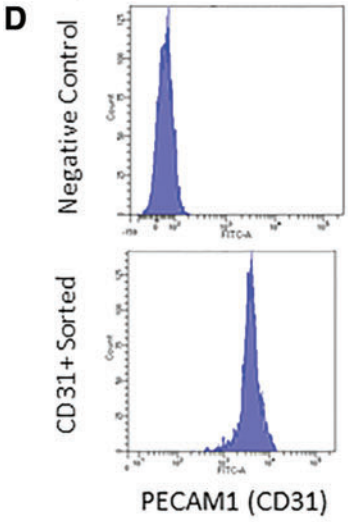

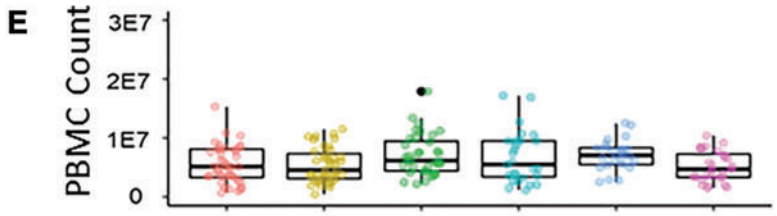

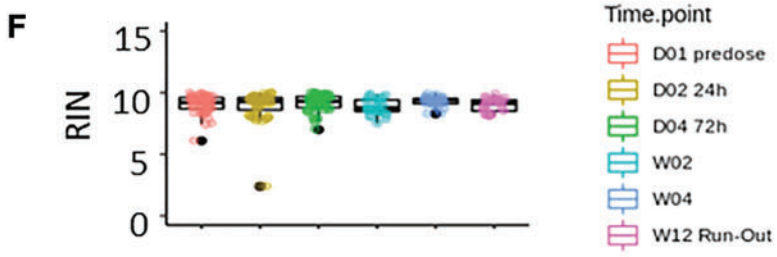

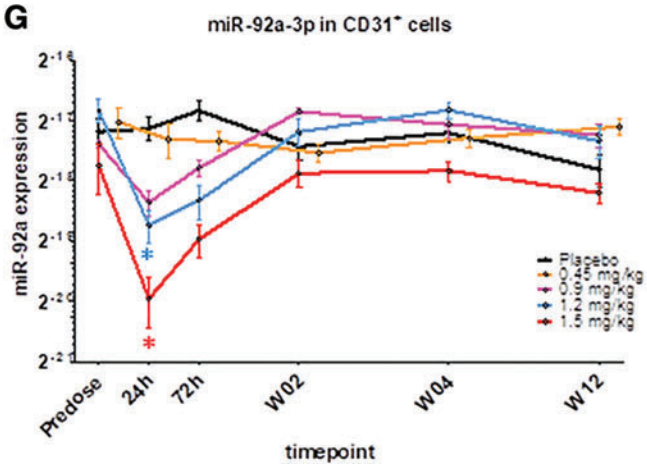

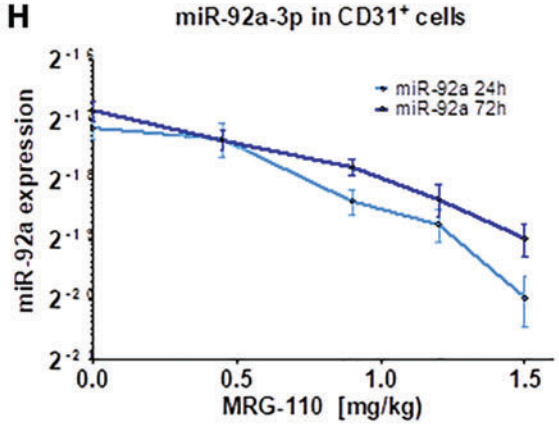

Regeneration for isolation of exosomes and $CD31^+$ cells. Samples arrived within 24 ± 12 h after collection.

ECV and $CD31^+$ cell isolation

After receipt of each delivery, for every time point, plasma was aliquoted from centrifuged samples to 2 mL DNA Low-Bind Eppendorf tubes. Plasma was centrifuged for ECV. Therefore, plasma aliquots were centrifuged at room temperature at 11,000 *g* for 2 min, then the supernatant was transferred to a new tube and centrifuged again at room temperature at 11,000 *g* for 2 min to deplete platelets and cell debris. Four milliliters of platelet poor plasma (supernatant) was transferred in ultracentrifuge tubes (4 mL/tube) in a prechilled TLA-110 rotor and was centrifuged at 100,000 *g* for 60 min at 4°C. The supernatant was aspirated and 700 μL Trizol was added to lyse the ECV, which were then stored at −80°C.

PBMCs were aliquoted to a 15-mL conical falcon tube containing the PBMC layer above the Ficoll plug. PBMCs were washed twice by centrifugation at 400 *g* for 5 min at room temperature in a swinging bucket centrifuge. The cell pellet was resuspended in 100 μL phosphate-buffered saline (PBS) and cell counts were obtained in a Neubauer chamber. PBMCs were frozen at 1×10^7 cells/mL aliquot in a screw-cap freezing tube [final solution EBM +10% dimethyl sulfoxide (DMSO) +20% fetal bovine serum (FBS)]. Aliquots were moved to CoolCell in a −80°C freezer.

For $CD31^+$ cell isolation, PBMCs were thawed in a 37°C water bath and washed in PBS. The cells were resuspended in 98 μL PBS and 2 μL Human Fc block was added for 10 min on ice. After washing, the cells were then resuspended in 80 μL PBS and 20 μL anti-CD31-FITC antibody and were incubated for 30 min on ice with occasional agitation. Cells were washed with PBS twice and resuspended in 80 μL PBS with 20 μL anti-FITC magnetic beads and incubated for 20 min on ice. Cells were washed twice and loaded onto a magnetic MS column as per the manufacturer's instructions (Miltenyi). The ''captured'' $CD31^+$ cell fraction was washed before lysing directly with 700 μL Trizol. The samples were stored at −80°C.

Before the phase 1 trial, a feasibility test was performed wherein blood from healthy ($n = 4$) volunteers was collected in Cell Preparation Tube (CPT) tubes and stored for delayed times to mimic shipping conditions. For ECV characteristic analysis, blood was collected and fractioned as described above using differential centrifugation methods. For these analyses, the pellet of the ultracentrifugation step was resuspended in 2 mL PBS for Nanosight Tracking Analysis (ECV size determination) using the manufacturer's guidelines for sample acquisition.

Sample analysis, methods for RNA lysate acquisition and quantification

Total RNA was isolated from each sample using the miRNeasy Mini Kit (No. 217004; Qiagen) according to the manufacturer's protocol. Automated electrophoresis of recovered RNA was assessed with an Agilent 2100 Bioanalyzer instrument (Agilent) using the Agilent RNA 6000 Pico Kit (5067-1513) or Agilent RNA 6000 Nano Kit (5067-1511), respectively. The same volume (1 μL) was tested from each sample, although varying RNA abundance was recovered from each isolation.

For isolated $CD31^+$ cells/exosomes, 10 μL of the eluted RNA was used. Samples and complementary DNA (cDNA) synthesis reagents were thawed on ice, gently vortexed to thoroughly mix, and then centrifuged briefly to eliminate air bubbles. Fifty percent PEG 8000 reagent was brought to room temperature for the adaptor ligation reaction. A 1.5-mL microcentrifuge tube, with sufficient Poly(A) Reaction Mix for the required number of reactions, was prepared according to the manufacturer's guidelines. The Poly(A) Reaction Mix was vortexed, and then centrifuged briefly to spin down the contents and eliminate air bubbles. Then, 2 μL of sample was added to each well of a reaction plate or each reaction tube, and then 3 μL of Poly(A) Reaction Mix was transferred to each well or tube. Then standard polyadenylation was performed and was immediately followed by adaptor ligation reaction according to the manufacturer's protocol. The Ligation Reaction Mix was transferred to each well of the reaction plate or each reaction tube containing the poly(A) tailing reaction product. After ligation, reverse transcription (RT) reaction immediately followed. RT Reaction Mix was prepared according to the manufacturer's protocol and 15 μL was transferred to each well of the reaction plate or each reaction tube containing the adaptor ligation reaction product. miR-Amp reaction was performed according to the manufacturer's protocol and transferred to each well of a new reaction plate or reaction tube. Next, 5 μL of the RT reaction product was used with a 1:10 dilution of cDNA template in $0.1 \times$ TE buffer. PCR Reaction Mix was transferred to each well of a PCR reaction plate and diluted. cDNA template was then added to each reaction well of the plate.

Thermal profiles were optimized for use with TaqMan® Fast Advanced Master Mix and were used with Fast reaction plates and the corresponding instrument block configurations. Use of relative quantification (ΔΔCt) method to analyze results was implemented. $CD31^+$ cell-derived RNA samples were run in triplicates. ECV were run in duplicate. miRNA or target mRNA concentrations were calculated using the standard $2^{-\Delta CT}$ (normalized) method.

scRNA-seq library preparation and analysis

Before $CD31^+$ isolation in the 1.5 mg/kg MRG-110 dose cohort, an aliquot of PBMCs was utilized for single-cell RNA sequencing library preparation. Cellular suspensions were loaded on a 10X Chromium Controller (10X Genomics) according to the manufacturer's protocol based on the 10X Genomics proprietary technology. Single-cell RNA-Seq libraries were prepared using Chromium Single-Cell 3′ Reagent Kit, v3 (10X Genomics), according to the manufacturer's protocol. Briefly, the initial step consisted of performing an emulsion capture where individual cells were isolated into droplets together with gel beads coated with unique primers bearing 10X cell barcodes, UMI (unique molecular identifiers), and poly(dT) sequences. RT reactions were engaged to generate barcoded full-length cDNA followed by the disruption of emulsions using the recovery agent and cDNA cleanup with DynaBeads MyOne Silane Beads (Thermo Fisher Scientific). Bulk cDNA was amplified using a Biometra Thermocycler TProfessional Basic Gradient with 96-Well Sample Block (98°C for 3 min; cycled 14×: 98°C for 15 s, 67°C for 20 s, and 72°C for 1 min; and 72°C for 1 min; held at 4°C). Amplified cDNA product was cleaned with the SPRIselect Reagent Kit (Beckman Coulter). Indexed sequencing libraries were constructed using the reagents from the Chromium Single-Cell 3′

v3 Reagent Kit as follows: fragmentation, end repair, and A-tailing; size selection with SPRIselect; adaptor ligation; postligation cleanup with SPRIselect; sample index PCR; and cleanup with solid phase reversible immobilization (SPRI) select beads. Library quantification and quality assessment were performed using Bioanalyzer Agilent 2100 using a High Sensitivity DNA chip (Agilent Genomics). Indexed libraries were equimolarly pooled and sequenced on two Illumina NovaSeq 6000 using paired-end 26×98 bp as sequencing mode.

Single-cell RNA sequencing data analyses

Single-cell expression data were processed using the Cellranger Software Suite (v. 3.1.0) to perform quality control, sample demultiplexing, and barcode processing. Sequencing reads were aligned to the human reference genome GRCh38 and afterward single-cell 3′ gene counting was performed using Starsolo (v. 2.7.3a), with default parameters. Dimensional reduction analysis was performed in Seurat (v3) in R (v3.6). The gene-cell-barcode matrix of the samples was log-transformed and filtered based on the number of genes detected per cell (any cell with <200 genes per cell was filtered out). Regression in gene expression was performed based on the number of UMI. Principal component analysis (PCA) was run on the normalized gene-barcode matrix. Barnes-hut approximation to t-stochastic neighbor embedding (t-SNE) was then performed on principal components to visualize cells in a two-dimensional space. This graph-based clustering method relies on a clustering algorithm based on shared nearest neighbor modularity optimization. Differential transcriptional profiles by cluster were generated in Seurat [16,17] with associated gene ontology terms derived from the functional annotation tools DAVID Bioinformatics Resources 6.7 (NIAID/NIH, https://david.ncifcrf.gov/summary.jsp) and Metascape [18] (http://metascape.org), and Enrichr tool (https://amp.pharm.mssm.edu/Enrichr). Cell annotation was then performed by assessing relative expression of immune markers as described in the Results section.

Statistical analysis

Analysis was performed with analysis of variance (repeated measures), or Student's *t*-test as indicated (GraphPad). Differential gene expression was determined using Seurat FindMarkers function, using a statistical test developed for single-cell data analysis (''bimod'' test) built within the Seurat package, accounting for dropout effects, and utilizing a combined likelihood ratio test for differential expression that incorporates discrete and continuous components. Differentially expressed genes were then cross-referenced with a list of predicted targets obtained from the miRDB [19] database (http://www.mirdb.org) for assessing putative target regulation. MiRDB targets are predicted by the bioinformatics tool MirTarget. Genes with adjusted *P* values <0.05 were considered differentially expressed genes. Adjusted *P* values were based on a Bonferroni correction to account for multiple testing.

Results

MRG-110 reduces miR-92a levels in whole blood and circulating CD31$^+$ cells

To determine the activity of MRG-110 in humans, we analyzed miR-92a levels in whole blood in healthy subjects being treated with a single intravenous dose of 0.01, 0.05, 0.15, 0.45, 0.9, 1.2, or 1.5 mg/kg MRG-110. MRG-110 dose and time dependently reduces miR-92a levels with a >95% inhibition achieved at 24 h after infusion of concentrations of 0.9 mg/kg and higher. A significant reduction of miR-92a was observed up to 2 weeks with concentrations of ≥0.9 mg/kg leading to a reduction of 43.9% ± 23.4%, 34.9% ± 32.7%, and 14.0% ± 13.5% compared to baseline levels in the 0.9-, 1.2-, and 1.5-mg/kg groups, respectively (Fig. 1B, C). At a lower concentration of 0.45 mg/kg, a significant inhibitory effect was observed at 24 h, resulting in miR-92a levels of 23.5% ± 5% compared to baseline levels. The calculated half-maximal inhibitory dose was 0.27 mg/kg at 24 h and 0.31 mg/kg at 72 h.

To gain further insights into the miR-92a inhibition within cells, which might be putative therapeutic targets, we isolated CD31$^+$ cells, which comprise monocytes, and circulating endothelial cells. CD31$^+$ cells were isolated by means of magnetic beads resulting in 96.9% positive events with a mean fluorescence intensity of 2,301 A.U. FACS analysis in a feasibility study demonstrated enrichment of CD31 (PECAM1) (Fig. 1D). Isolated RNA achieved an average RNA Integrity Number (RIN) of 9.0 ± 0.90 A.U., with no significant change between time points after MRG-110 administration for RIN scores or PBMC counts (Fig. 1E, F). Measurement of miR-92a levels in isolated CD31$^+$ cells showed similar trends as in whole blood; however, significant inhibition was only observed at concentration of ≥1.2 mg/kg at 24 h (Fig. 1G, H).

MRG-110 reduces miR-92a expression in ECV

Next, we assessed the effect of MRG-110 treatment on miR-92a levels in circulating ECV, which are known to be mainly released by circulating cells, particularly platelets, and endothelial cells [20]. Therefore, we used published protocols [21,22] to isolate ECV from platelet-free plasma. Vesicles had a mean diameter of 184.3 ± 6.9 nm, which was not altered by delay of the isolation in a test run for 24 to 48 h to mimic sample shipping timelines ($n = 4$ healthy volunteers, data not shown). MRG-110 reduced miR-92a levels in isolated ECV, with a significant reduction detected in the 0.9 and 1.5 mg/kg group and a trend ($P = 0.09$) observed 24 h after infusion of 1.2 mg/kg (Fig. 2A). The inhibitory effect lasted up to 72 h in the high-dose group (Fig. 2B). To get insights whether MRG-110 treatment might have affected the compilation of the ECV, we additionally measured miR-126, which is highly expressed in endothelial cells and platelet-derived exosomes. However, miR-126 levels were not affected by the treatment (Fig. 2C).

MRG-110 treatment derepresses target genes in circulating cells

To gain further insights into the functional downstream effects achieved by MRG-110 in humans, we determined the expression of miR-92a targets. First, we determined the expression of *ITGA5*, which is a well-established and validated target [5] by measuring mRNA expression in whole blood. *ITGA5* mRNA time dependently increased in subjects of the high-dose group (1.5 mg/kg) compared to placebo (Fig. 3A). The effect was dose dependent, but significant derepression was only observed in the 1.5 mg/kg group at 4 weeks (Fig. 3B). In addition, *CD93*, which was validated as a miR-92a target in wound healing [6], was derepressed after MRG-110 treatment

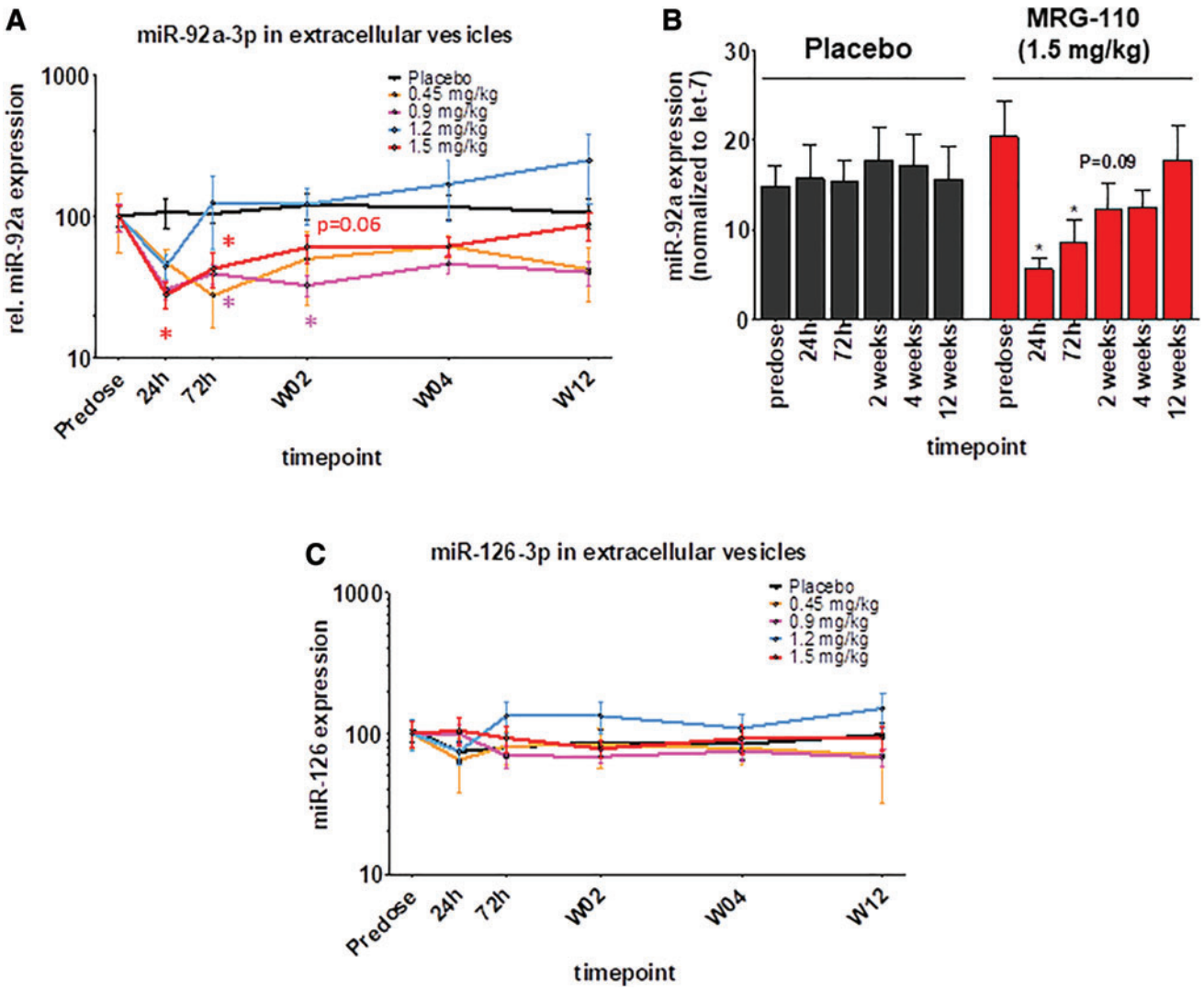

FIG. 2. MRG-110 reduces expression of miR-92a-3p in extracellular vesicles. **(A)** Expression of miR-92a-3p (normalized to let-7g) in isolated extracellular vesicles of subjects treated with a single intravenous infusion of MRG-110. $N = 5$ in each treatment group, $N = 14$ subjects in placebo. $^*P < 0.05$ versus placebo. Student's *t*-test. $P < 0.05$ for group comparison, 0.9 and 1.5 mg/kg group by ANOVA. **(B)** Expression of miR-92a-3p in isolated extracellular vesicles (normalized to let-7g) from patients with injection of placebo or MRG-110. $N = 5$ in each treatment group, $N = 14$ subjects in placebo. $^*P < 0.05$ ANOVA multiple groups. **(C)** Expression of miR-126 (normalized to let-7g) in isolated extracellular vesicles of subjects treated with a single intravenous infusion of MRG-110. $N = 5$ in each treatment group, $N = 14$ subjects in placebo. ANOVA, analysis of variance. Color images are available online.

with similar kinetics as *ITGA5* (Fig. 3C, D). The other previously identified targets *ERGIC2* and *MAN2A1* [6] were not regulated in whole blood (Fig. 3E, F).

Since miRNA targets can be cell type specific due to differences in mRNA expression levels, splice variants, and/or RNA binding protein pattern [23], which may mask miR binding sites in 3′ untranslated regions (UTRs), we additionally assessed the transcriptome in frozen PBMCs isolated at baseline and after 72 h of treatment with 1.5 mg/kg MRG-110. Clustering of the total cells revealed seven major clusters, which could be assigned to NK cells, CD4 and CD8 T cells, B cells, and smaller clusters of $FCGR3A^+$ and $CD14^+$ monocytes and plasma cells (Fig. 4A). The expression of marker genes characterizing the individual clusters is shown in Supplementary Fig. S1. The individual clusters were similarly populated by cells isolated from the predose and postdose group (Fig. 4B).

To gain insights into the regulation of miR-92a targets, we first analyzed the expression in the total cell population (Supplementary Fig. S2). As shown by the heatmap, anti-miR-92a treatment significantly derepressed many predicted miR-92a targets (Supplementary Fig. S2). Next, we selected all *in silico* predicted targets and determined their expression in the individual clusters. NK cells and CD4 or CD8 T cells showed the most prominent changes in predicted miR-92a targets (Fig. 4D). Interestingly, *MAN1A1*, a family member of *MAN2A1*, which is a validated target in wound healing, but was not regulated in whole blood, was significantly induced in NK cells (Fig. 4D). In addition, several other genes, which were reported to be involved in NK cell maturation or

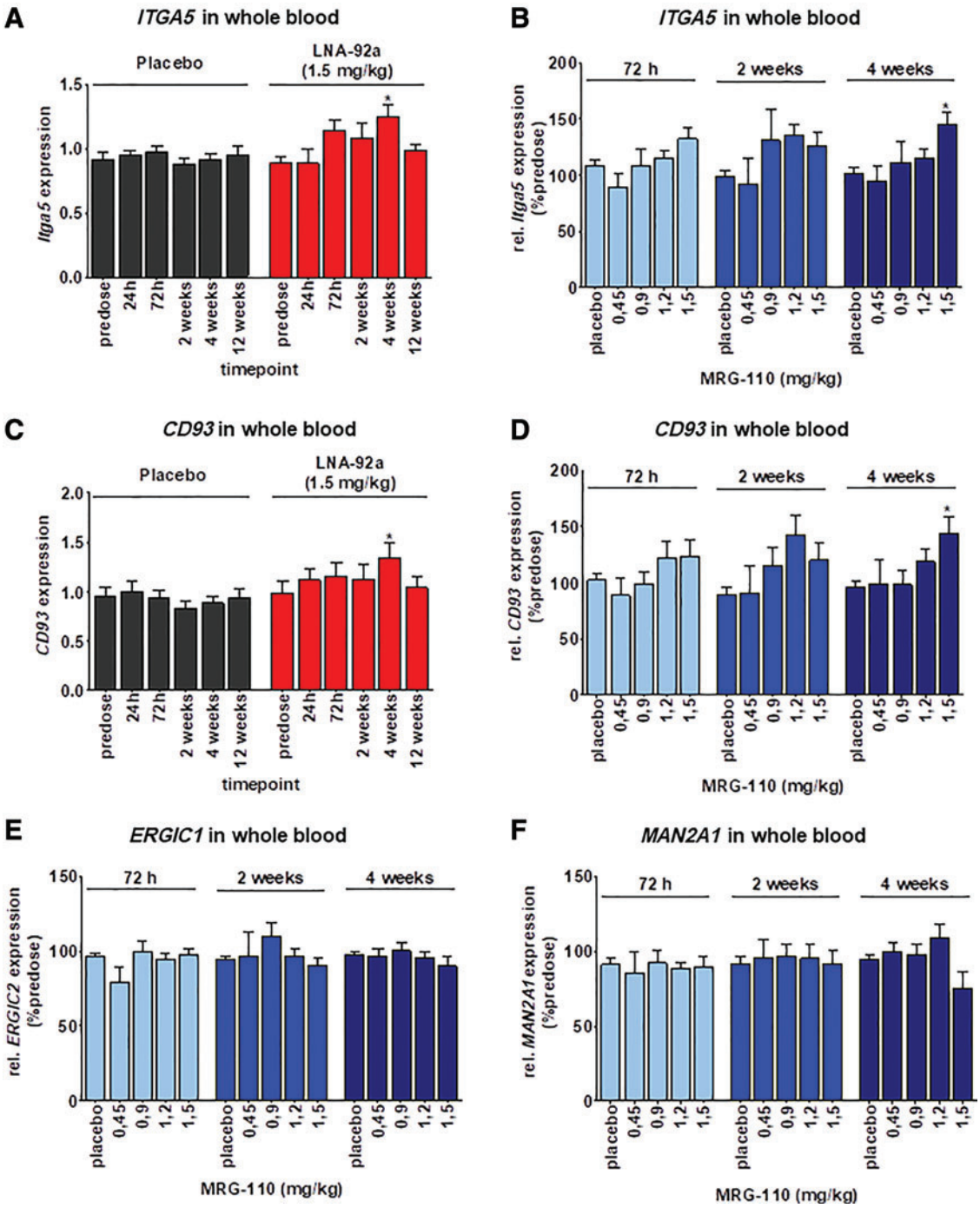

FIG. 3. MRG-110 regulates some miR-92a target genes in whole blood. **(A–F)** Effect of single infusion of MRG-110 on mRNA expression of miR-92a target genes in whole blood. $N = 5$ in each treatment group, $N = 14$ subjects in placebo group. $P < 0.05$ versus predose (ANOVA). mRNA, messenger RNA. Color images are available online.

FIG. 4. MRG-110 regulated diverse predicted miR-92a targets in single-cell RNA sequencing of total PBMCs. **(A)** t-SNE plot showing the clustering of respective blood cells. Predose: 4,945 cells; Postdose: 2,684 cells (72 h after 1.5 mg/kg MRG-110 treatment). For further details regarding marker genes used for annotation, see Supplementary Fig. S1B. Contribution to cells from the predose or postdose group. No significant differences were seen. **(C)** Number of total differentially expressed genes (predose vs. postdose) in the different cell clusters. **(D–F)** Violin plots showing expression of predicted miR-92a target genes in NK cells **(D)**, $CD4^+$ cells **(E).** and $CD8^+$ cells **(F)**. $^*P < 0.05$ versus predose. t-SNE, t-stochastic neighbor embedding. Color images are available online.

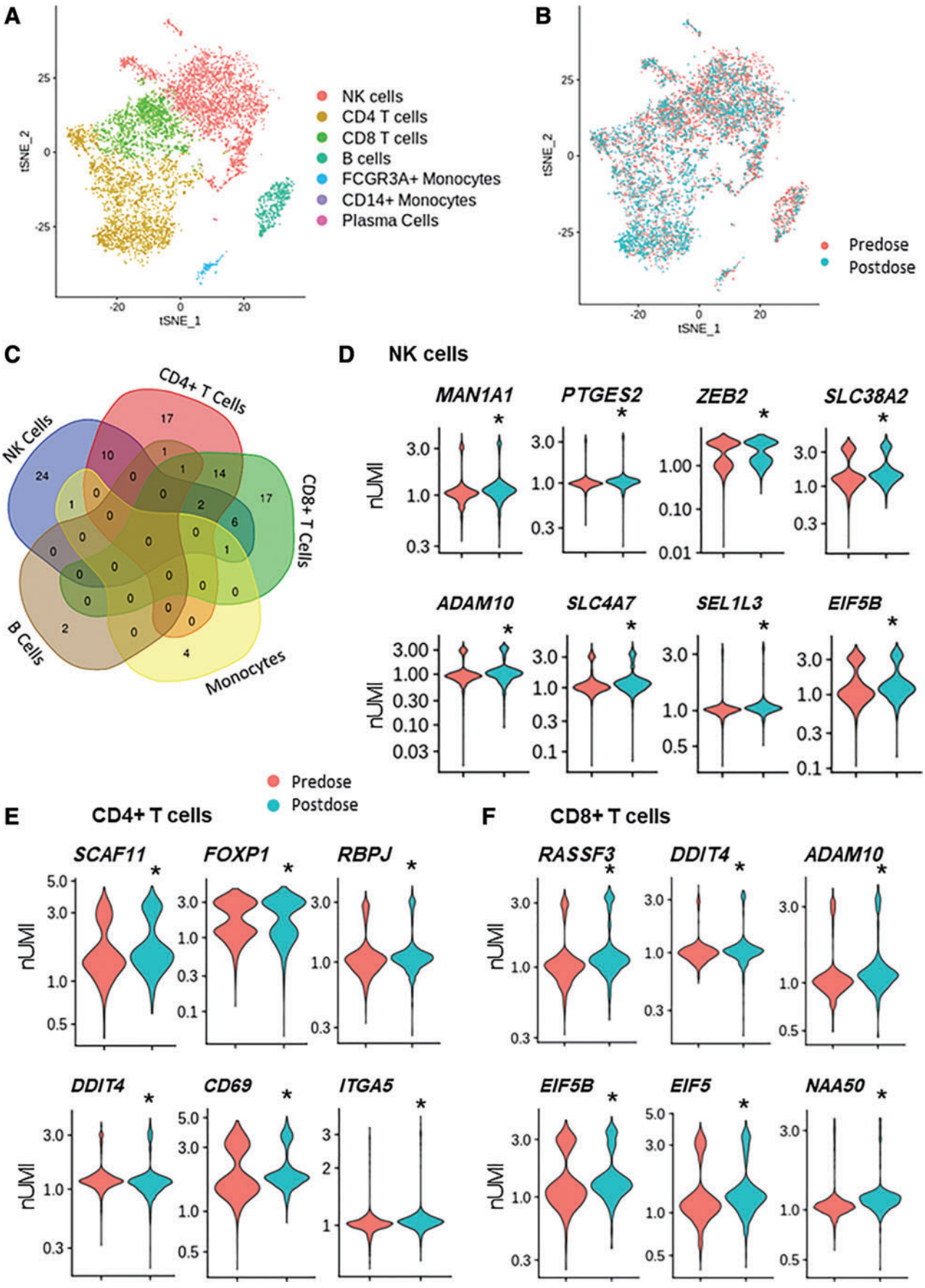

function, were derepressed. These genes include *ZEB2*, which controls NK cell maturation and rejection of melanoma cells [24], *ADAM10*, which has been shown to contribute to NK cell expansion [25], and the sodium- and bicarbonate-dependent cotransporters *SLC4A7* and *SLC38A2*, with *SLC38A2* being the predominant system L-amino acid transporter in activated NK cells [26]. In $CD4^+$ T cells, MRG-110 increased the expression of 17 genes, including the SR-related CTD-associated factor 11 (SCAF11), FoxP1, a regulator of T cell quiescence [27], DDIT4 (also known as REDD1), which modulates TH17 and T cell proliferation [28], and CD69, which is implicated in T cell differentiation as well as lymphocyte retention in lymphoid organs (Fig. 4E). $CD8^+$ T cells of MRG-110-treated humans also showed increased DDIT4 and ADAM10 levels, which were also seen upregulated in $CD4^+$ and NK cells, respectively. MRG-110 further upregulated the tumor suppressor RASSF5 and the translation initiation factors EIF5 and EIF5A. These data demonstrate that administration of MRG-110 in humans significantly interferes with immune cell-associated gene expression (Fig. 4F).

Discussion

This study reports that single dosing of MRG-110 efficiently reduced miR-92a levels in the peripheral blood compartment in humans. The half -maximal dose in whole blood was between 0.27 and 0.31 mg/kg, which is lower than previously reported dosages of other anti-miRs. For example, miravirsen was reported to have a half-maximal dose of 10 mg/kg in mice and about 3 mg/kg in non-human primates [29]. A weekly dosing of at least 5 mg/kg was necessary to detect a significant effect on the target in humans [4]. Similar dose levels of cobomarsen, 300–900 mg/dose given on a weekly schedule, were used in a Phase 1 clinical trial of cutaneous T cell lymphoma patients [15]. The relatively high efficiency of MRG-110 in humans compared to other anti-miRs in humans is consistent with the preclinical finding that intracoronary infusion of 0.03–0.15 mg/kg anti-miR-92a (with the same formulation as MRG-110) in pigs increased the recovery after acute myocardial infarction [12]. However, intracoronary infusion leads to an enrichment of MRG-110 by approximately six-fold in the myocardium, suggesting that the local therapeutic effects in tissue may not necessarily be directly comparable to the systemic effects. When measuring miR-92a expression in isolated cells or ECV in this study, significant effects on miR-92a expression levels were observed only in the higher dose groups of >0.9 mg/kg, which may suggest measuring of the targeted miRNA by PCR in whole blood overestimates the biological effects due to possible interference of the remaining anti-miR in the sample. Alternatively, one may speculate that intracellular uptake and efficient functional blocking of miR-92a in exosomes or cells, which derive from bone marrow or tissue, may require higher doses compared to what is seen in whole blood. This is consistent with the finding that target derepression was only detected in the 1.5 mg/kg cohort. Overall, these data point to MRG-110 being a very potent anti-miR compared to many previously tested substances, which usually are effective at concentrations of >5 mg/kg. However, given the differences in readouts, target tissues, and cells, as well as length of anti-miRs, the potential differences in potency are currently being investigated.

Our study confirmed the regulation of some of the known and well-established miR-92a target genes such as *ITGA5* and *CD93* in whole blood of humans. Some other targets, such as *ERGIC* and *MAN2A1*, were, however, not regulated. Since these targets have been established in other tissues (specifically in the skin), the lack of regulation may reflect a cell type-specific effect of miR-92a. Since the efficiency of miRNA targeting is affected by many factors, including the level of target gene expression, the isoform of the 3′ UTR, and the expression of RNA binding proteins, which can interfere with the miRNA binding sites, such cell type-specific effects can be expected. Indeed, in the heart, anti-miR-92a treatment elicited striking cell type-specific effects with only the minority of targets being derepressed in all cell types [23]. MiR-92a also showed different effects in a study comparing different cell lines [30]. We, therefore, additionally used single-cell sequencing to determine the effect of miR-92a inhibition on the different cell populations in the blood. Our data demonstrate that MRG-110 significantly affects many predicted targets in NK cells and CD4 and CD8 T cells. The microRNA-17-92 cluster is well known to regulate immune cell functions: it was first found in malignant B cell lymphoma and was shown to promote early B cell development and production of IgM antibodies after antigen stimulation [31]. The miR-17-92 cluster is also involved in T cell activation and promotes Th1 and Th2 responses, whereas the role in NK cells is unknown [32]. Surprisingly, little is known regarding the specific influence of miR-92a on immune cell functions. MiR-92a appears enriched in naive T cells [33]. Furthermore, miR-92a was reported to be upregulated in experimental autoimmune encephalomyelitis [34], in which IFN-γ-producing Th1 cells are major players. Overexpression of miR-92a led to increased differentiation of Th1 cells, which may contribute to the pathological development of this autoimmune disease [34].

The differential gene expression patterns observed in T cells of MRG-110-treated subjects are in line with these studies. Elevated *DDIT4* levels in $CD4^+$ T cells may have interesting implications for maintenance of T cell differentiation and homeostasis. Reports demonstrate that DDIT4 is essential for control of autophagy [35] as well as optimal T cell proliferation and survival [36]. Importantly, *RBPJ* upregulation may play a key role in maintaining, if not decreasing, Th17/Treg ratios and still elevated *FOXP1* levels may indicate enhanced regulation of quiescence in $CD4^+$ T cells [27]. Together, the regulation of these genes by MRG-110 may be a stabilizing mechanism, which facilitates wound healing through diminished autoreactivity and altered Th17 differentiation.

In addition, derepression of genes like *ADAM10* in NK cells may have interesting implications. While ADAM10 is needed for NK proliferation, hypoxia-induced HIF-1a is also associated with elevated metalloproteinases like ADAM10, which facilitates tissue growth, in part, through diminished immune surveillance [37]. However, the lack of a detailed immune profiling and functional assays in our study precludes further conclusions regarding T cell and NK cell responses.

In conclusion, MRG-110 treatment results in reduced miR-92a levels and de-repression of gene targets in human peripheral blood cells. The most striking effect regarding target gene expression was detected in T cells, specifically NK

cells. NK cells are a part of the innate immune response that contributes to the eradication of virus-infected cells and cancer cells by natural cytotoxicity and production of immune-modulatory cytokines. Therefore, our findings may raise the hypothesis that miR-92a interferes with immune responses and T cell functions in humans, which provide the basis to further explore a therapeutic benefit in diseases with dysregulated immune functions.

Acknowledgment

We would like to thank Katrin Häfner for expert technical support.

Author Disclosure Statement

S.D. and A.Z. have a patent on miR-92a targeting in cardiovascular disease. S.D. has a research contract with Servier and is scientific advisor of miRagen Therapeutics. W.G., H.D., G.A., I.P., F.F. are employees of Servier, R.M. and L.P. are employees of miRagen Therapeutics. All other authors have no competing financial interests.

Funding Information

The study was supported by the German Center for Cardiovascular Research (DZHK), the Leducq Network MIR-VAD, and the Rolf M. Schwiete foundation.

Supplementary Material

Supplementary Figure S1
Supplementary Figure S2

References

1. Lucas T, A Bonauer and S Dimmeler. (2018). RNA therapeutics in cardiovascular disease. Circ Res 123:205–220.
2. van Rooij E and S Kauppinen. (2014). Development of microRNA therapeutics is coming of age. EMBO Mol Med 6:851–864.
3. Krutzfeldt J, N Rajewsky, R Braich, KG Rajeev, T Tuschl, M Manoharan and M Stoffel. (2005). Silencing of microRNAs in vivo with ''antagomirs.'' Nature 438:685–689.
4. Janssen HL, HW Reesink, EJ Lawitz, S Zeuzem, M Rodriguez-Torres, K Patel, AJ van der Meer, AK Patick, A Chen, *et al.* (2013). Treatment of HCV infection by targeting microRNA. N Engl J Med 368:1685–1694.
5. Bonauer A, G Carmona, M Iwasaki, M Mione, M Koyanagi, A Fischer, J Burchfield, H Fox, C Doebele, *et al.* (2009). MicroRNA-92a controls angiogenesis and functional recovery of ischemic tissues in mice. Science (80–) 324:1710–1713.
6. Gallant-Behm CL, J Piper, BA Dickinson, CM Dalby, LA Pestano and AL Jackson. (2018). A synthetic microRNA-92a inhibitor (MRG-110) accelerates angiogenesis and wound healing in diabetic and nondiabetic wounds. Wound Repair Regen 26:311–323.
7. Lucas T, F Schafer, P Muller, SA Eming, A Heckel and S Dimmeler. (2017). Light-inducible antimiR-92a as a therapeutic strategy to promote skin repair in healing-impaired diabetic mice. Nat Commun 8:15162.
8. Daniel JM, D Penzkofer, R Teske, J Dutzmann, A Koch, W Bielenberg, A Bonauer, RA Boon, A Fischer, *et al.* (2014). Inhibition of miR-92a improves re-endothelialization and prevents neointima formation following vascular injury. Cardiovasc Res 103:564–572.
9. Hinkel R, D Penzkofer, S Zuhlke, A Fischer, W Husada, QF Xu, E Baloch, E van Rooij, AM Zeiher, C Kupatt and S Dimmeler. (2013). Inhibition of microRNA-92a protects against ischemia/reperfusion injury in a large-animal model. Circulation 128:1066–1075.
10. Loyer X, S Potteaux, AC Vion, CL Guerin, S Boulkroun, PE Rautou, B Ramkhelawon, B Esposito, M Dalloz, *et al.* (2014). Inhibition of microRNA-92a prevents endothelial dysfunction and atherosclerosis in mice. Circ Res 114:434–443.
11. Wu W, H Xiao, A Laguna-Fernandez, G Villarreal, Jr., KC Wang, GG Geary, Y Zhang, WC Wang, HD Huang, *et al.* (2011). Flow-dependent regulation of Kruppel-like factor 2 is mediated by microRNA-92a. Circulation 124:633–641.
12. Hinkel R, D Penzkofer, S Zühlke, A Fischer, W Husada, Q-F Xu, E Baloch, E van Rooij, AM Zeiher, C Kupatt and S Dimmeler. (2013). Inhibition of microRNA-92a protects against ischemia/reperfusion injury in a large-animal model. Circulation 128:1066–1075.
13. Bellera N, I Barba, A Rodriguez-Sinovas, E Ferret, MA Asin, MT Gonzalez-Alujas, J Perez-Rodon, M Esteves, C Fonseca, *et al.* (2014). Single intracoronary injection of encapsulated antagomir-92a promotes angiogenesis and prevents adverse infarct remodeling. J Am Hear Assoc 3: e000946.
14. Henique C, G Bollee, X Loyer, F Grahammer, N Dhaun, M Camus, J Vernerey, L Guyonnet, F Gaillard, *et al.* (2017). Genetic and pharmacological inhibition of microRNA-92a maintains podocyte cell cycle quiescence and limits crescentic glomerulonephritis. Nat Commun 8:1829.
15. Querfeld C, F Foss, Y Kim, L Pinter-Brown, B William, P Porcu, T Pacheco, B Haverkos, J DeSimone, *et al*. (2019). Phase 1 trial of cobomarsen, an inhibitor of miR-155, in cutaneous T-cell lymphoma. Clin Adv Hematol Oncol 17: 16–17.
16. Stuart T, A Butler, P Hoffman, C Hafemeister, E Papalexi, WM Mauck, 3rd, Y Hao, M Stoeckius, P Smibert and R Satija. (2019). Comprehensive integration of single-cell data. Cell 177:1888.e21–1902.e21.
17. Butler A, P Hoffman, P Smibert, E Papalexi and R Satija. (2018). Integrating single-cell transcriptomic data across different conditions, technologies, and species. Nat Biotechnol 36:411–420.
18. Zhou Y, B Zhou, L Pache, M Chang, AH Khodabakhshi, O Tanaseichuk, C Benner and SK Chanda. (2019). Metascape provides a biologist-oriented resource for the analysis of systems-level datasets. Nat Commun 10:1523.
19. Liu W and X Wang. (2019). Prediction of functional microRNA targets by integrative modeling of microRNA binding and target expression data. Genome Biol 20:18.
20. Brahmer A, E Neuberger, L Esch-Heisser, N Haller, MM Jorgensen, R Baek, W Mobius, P Simon and E-M Kramer-Albers. (2019). Platelets, endothelial cells and leukocytes contribute to the exercise-triggered release of extracellular vesicles into the circulation. J Extracell Vesicles 8: 1615820.
21. Boulanger CM, A Scoazec, T Ebrahimian, P Henry, E Mathieu, A Tedgui and Z Mallat. (2001). Circulating microparticles from patients with myocardial infarction cause endothelial dysfunction. Circulation 104:2649–2652.
22. Raposo G, HW Nijman, W Stoorvogel, R Liejendekker, CV Harding, CJ Melief and HJ Geuze. (1996). B lymphocytes

secrete antigen-presenting vesicles. J Exp Med 183:1161–1172.
23. Rogg E-M, WT Abplanalp, C Bischof, D John, MH Schulz, J Krishnan, A Fischer, C Poluzzi, L Schaefer, *et al.* (2018). Analysis of cell type-specific effects of microRNA-92a provides novel insights into target regulation and mechanism of action. Circulation 138:2545–2558.
24. van Helden MJ, S Goossens, C Daussy, A-L Mathieu, F Faure, A Marcais, N Vandamme, N Farla, K Mayol, *et al.* (2015). Terminal NK cell maturation is controlled by concerted actions of T-bet and Zeb2 and is essential for melanoma rejection. J Exp Med 212:2015–2025.
25. Pham D-H, J-S Kim, S-K Kim, D-J Shin, N-T-T Uong, H Hyun, MS Yoon, SJ Kang, YJ Ryu, *et al.* (2017). Effects of ADAM10 and ADAM17 inhibitors on natural killer cell expansion and antibody-dependent cellular cytotoxicity against breast cancer cells in vitro. Anticancer Res 37:5507–5513.
26. Loftus RM, N Assmann, N Kedia-Mehta, KL O'Brien, A Garcia, C Gillespie, JL Hukelmann, PJ Oefner, AI Lamond, *et al.* (2018). Amino acid-dependent cMyc expression is essential for NK cell metabolic and functional responses in mice. Nat Commun 9:2341.
27. Garaud S, F Roufosse, P De Silva, C Gu-Trantien, J-N Lodewyckx, H Duvillier, S Dedeurwaerder, M Bizet, M Defrance, *et al.* (2017). FOXP1 is a regulator of quiescence in healthy human CD4(+) T cells and is constitutively repressed in T cells from patients with lymphoproliferative disorders. Eur J Immunol 47:168–179.
28. Zhang F, G Liu, D Li, C Wei and J Hao. (2018). DDIT4 and associated lncDDIT4 modulate Th17 differentiation through the DDIT4/TSC/mTOR pathway. J Immunol 200: 1618–1626.
29. Elmen J, M Lindow, S Schutz, M Lawrence, A Petri, S Obad, M Lindholm, M Hedtjarn, HF Hansen, *et al.* (2008). LNA-mediated microRNA silencing in non-human primates. Nature 452:896–899.
30. Kohram F, P Fallah, M Shamsara, Z Bolandi, M Rassoulzadegan, M Soleimani and H Ghanbarian. (2018). Cell type-dependent functions of microRNA-92a. J Cell Biochem 119:5798–5804.
31. Ventura A, AG Young, MM Winslow, L Lintault, A Meissner, SJ Erkeland, J Newman, RT Bronson, D Crowley, *et al.* (2008). Targeted deletion reveals essential and overlapping functions of the miR-17 through 92 family of miRNA clusters. Cell 132:875–886.
32. Kuo G, C-Y Wu and H-Y Yang. (2019). MiR-17-92 cluster and immunity. J Formos Med Assoc 118:2–6.
33. Ohyashiki M, JH Ohyashiki, A Hirota, C Kobayashi and K Ohyashiki. (2011). Age-related decrease of miRNA-92a levels in human $CD8^+$ T-cells correlates with a reduction of naive T lymphocytes. Immun Ageing 8:11.
34. Rezaei N, F Talebi, S Ghorbani, A Rezaei, A Esmaeili, F Noorbakhsh and MG Hakemi. (2019). MicroRNA-92a drives Th1 responses in the experimental autoimmune encephalomyelitis. Inflammation 42:235–245.
35. Molitoris JK, KS McColl, S Swerdlow, M Matsuyama, M Lam, TH Finkel, S Matsuyama and CW Distelhorst. (2011). Glucocorticoid elevation of dexamethasone-induced gene 2 (Dig2/RTP801/REDD1) protein mediates autophagy in lymphocytes. J Biol Chem 286:30181–30189.
36. Reuschel EL, J Wang, DK Shivers, K Muthumani, DB Weiner, Z Ma and TH Finkel. (2015). REDD1 is essential for optimal T cell proliferation and survival. PLoS One 10: e0136323.
37. Barsoum IB, TK Hamilton, X Li, T Cotechini, EA Miles, DR Siemens and CH Graham. (2011). Hypoxia induces escape from innate immunity in cancer cells via increased expression of ADAM10: role of nitric oxide. Cancer Res 71:7433–7441.

Address correspondence to:
Stefanie Dimmeler, PhD
Institute for Cardiovascular Regeneration
Centre of Molecular Medicine
Goethe University Frankfurt
Theodor Stern Kai 7
60590 Frankfurt
Germany

E-mail: dimmeler@em.uni-frankfurt.de

Received for publication April 16, 2020; accepted after revision June 18, 2020; Published Online July 20, 2020.